Nanoscale

PAPER

View Article Online
View Journal | View Issue

Cite this: *Nanoscale*, 2019, **11**, 13800

Published on 27 June 2019. Downloaded by Radboud University Nijmegen on 8/13/2019 10:43:32 AM.

Effects of out-of-plane strains and electric fields on the electronic structures of graphene/MTe (M = Al, B) heterostructures†

Dingbo Zhang, *[a,b,c] Yue Hu,[a] Hongxia Zhong,[b] Shengjun Yuan[b] and Chang Liu[b]

Received 20th May 2019,
Accepted 27th June 2019

DOI: 10.1039/c9nr04287c

rsc.li/nanoscale

Contacts between graphene and two-dimensional (2D) semiconductors have been widely investigated because of their tunable Schottky barrier height (SBH) by means of applied out-of-plane strains, electric fields, *etc*. Here, based on first-principles calculations, we study the effects of out-of-plane strains (a tensile or compressive strain) and electric fields on the electronic structures of graphene/MTe (M = Al, B) heterostructures. The calculated results indicate that p-type Schottky barriers are formed at the graphene/AlTe and graphene/BTe interfaces with 0.72 and 0.49 eV, respectively. The increase in the interlayer distances (tensile strains) between graphene and MTe can induce a transition from a p-type to n-type Schottky contact. On the other hand, the decrease in the interlayer distances (compressive strains) can transform graphene/MTe into semiconductors, which originates from graphene/MTe with a large compressive strain that makes the two carbon sublattices inequivalent, inducing a band gap. In addition, the applied electric fields can modulate effectively the contact formation (a Schottky or Ohmic contact) and the doping of graphene in graphene/MTe heterostructures. Our study suggests two facile methods to tune the electronic properties of graphene/MTe heterostructures and offer a possibility for graphene/MTe heterostructure-based electronic devices.

Introduction

Graphene, a one-atom-thick two-dimensional (2D) layer of sp^2-hybridized carbon, has become one of the hottest topics in the fields of materials science due to its remarkable physical properties such as a high carrier mobility up to 10^6 cm^2 V^{-1} s^{-1}, the Dirac cone-like structure, excellent optical transmittance and exceptional mechanical strength.[1–3] Nevertheless, the absence of an electronic band gap and fast carrier recombination limits its application in nano-electronic systems.[4,5] Constructing heterostructures by combining graphene with various functional 2D materials is a powerful strategy to expand the applied scope of graphene.[6] For example, graphene/metal shows low contact resistance,[7] graphene/WSe_2 has ambipolar characteristics,[8] graphene/MoS_2 has been used in memory devices with the on/off current ratio being tuned to be up to 100,[9] and graphene/phosphorene is a potential candidate for further energy storage devices.[10] These graphene-based heterostructures possess Dirac cone-like structure, low contact resistance and many other novel optoelectronic properties far beyond individual components, which can greatly promote the development of graphene-based applications.

Under normal conditions, graphene-based semimetal–semiconductor heterostructures form Schottky or Ohmic contacts at the interfaces.[11] The charge transfer easily occurs at the interfaces because of different work functions W_F (the difference between the vacuum level E_{vacuum} and the Fermi level E_f).[3] In the view of the Schotty–Mott model,[12] the n-type Schottky barrier Φ_n is the energy difference between the conduction band minimum (CBM) E_c and the Fermi level E_f ($\Phi_n = E_c - E_f$). Similarly, the p-type Schottky barrier Φ_p is the energy difference between the Fermi level E_f and the valence band minimum (VBM) E_v ($\Phi_p = E_f - E_v$). When Φ_n or Φ_p becomes a negative value, an Ohmic contact will be formed at the interfaces. The controllable Schottky barrier height (SBH) is a crucial factor for the efficient operation of electronic devices.[13,14] Previous reports show that in graphene/GaN,[15] graphene/MoS_2,[16] graphene/GaSe,[17] graphene/SnS[18] and graphene/$X(OH)_2$ (X = Ca, Mg),[19] the SBH can be modulated by the applied out-of-plane strains or applied external electric fields.

[a]School of Physical Science and Technology, Key Laboratory of Advanced Technologies of Materials, Ministry of Education of China, Southwest Jiaotong University, Chengdu 610031, China. E-mail: 741220395@qq.com
[b]Key Laboratory of Artificial Micro- and Nano-Structures of Ministry of Education and School of Physics and Technology, Wuhan University, Wuhan 430072, China
[c]Henan Key Laboratory of Photovoltaic Materials, and School of Physics and Materials Science, Henan Normal University, Xinxiang 453007, China

†Electronic supplementary information (ESI) available. See DOI: 10.1039/c9nr04287c

This journal is © The Royal Society of Chemistry 2019

Published on 27 June 2019. Downloaded by Radboud University Nijmegen on 8/13/2019 10:43:32 AM.

Recently, the two-dimensional structures of group III–VI monolayers, MX (M = B, Al, Ga, In and X = O, S, Se, Te) have been predicted theoretically to the geometry of monolayer GaS, which have been synthesized.[20] The structures of MX consist of a four-atom basis in a unit cell with four layers in the order of the X–M–M–X stacking, belonging to the space group D_{3h}.[21] To the best of our knowledge, no work has been reported on the electronic properties and Schottky contacts of graphene/MTe (M = Al, B).

In this paper, we build graphene/MTe heterostructures and investigate their electronic structures. Our density functional calculations indicate that the graphene/MTe vdW heterostructures form p-type Schottky contacts. Both applied out-of-plane strains and applied external electric fields can modulate the SBH. Furthermore, the tunable doping type and tunable charge carrier concentrations of graphene in the graphene/MTe heterostructures can be achieved by the applied electric fields.

Computational methods

Density functional theory (DFT) calculations were carried out by using the Vienna *Ab initio* Simulation Package (VASP).[22,23] We employed the generalized gradient approximation (GGA) with the Perdew–Burke–Ernzerhof (PBE) parameterization to describe electron exchange and correlation effects.[24] The semi-empirical DFT-D2 method was used to correct the vdW interaction in 2D systems.[25] For all geometry relaxation, the shape and lattice parameters of the supercell remained unchanged, and the atoms were allowed to fully relax. All atomic positions were relaxed until the maximal residual force per atom and the energy difference were less than 10^{-2} eV Å^{-1} and 10^{-5} eV, respectively. A cutoff energy of 500 eV and a 7 × 7 × 1 *k*-point mesh for the first Brillouin zone integration were utilized.[24] To avoid the interactions between the adjacent slabs, a vacuum region of at least 20 Å was used in our calculations.[26]

Results and discussion

Geometry structures of graphene/MTe (M = Al, B) heterostructures

The optimized lattice constants of graphene, AlTe and BTe unit cells are a_g = 2.46 Å, a_{AlTe} = 4.25 Å and a_{BTe} = 3.56 Å, respectively, which are in good agreement with those reported in previous studies.[21,27] Meanwhile, the thermodynamical stability of AlTe and BTe monolayers are again evaluated by calculating phonon dispersion. No imaginary frequency was observed in the two phonon spectra, as demonstrated in Fig. S1(a and b) (ESI†), which indicates that both AlTe and BTe are stable. However, there is a large difference of about 40% (30%) in the lattice constants between graphene and AlTe (BTe). A $\sqrt{3} \times \sqrt{3} \times 1$ graphene and 1 × 1 × 1 AlTe supercell therefore are used to build a graphene/AlTe system, while a 3 × 3 × 1 graphene and 2 × 2 × 1 BTe supercell are used to construct a graphene/BTe heterostructure, as shown in Fig. 1.

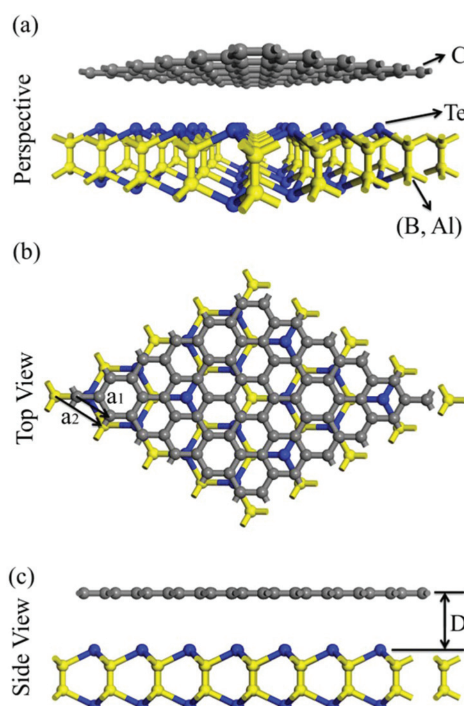

Fig. 1 Perspective, top and side views of the graphene/MTe heterostructures. The lattice constants of graphene and MTe are a_1 and a_2, respectively. *D* represents the equilibrium distance between graphene and MTe. The gray, yellow and blue balls denote carbon, M and Te atoms, respectively.

Meanwhile, the average lattice constant is considered to minimize the lattice mismatch. The lattice mismatch between graphene and AlTe (BTe) is only 0.1% (1.7%) and has little effect on our calculation results. Then, we investigated several possible configurations of graphene/XTe heterostructures (see Fig. S2(a–f) and S3(a–f) (ESI†)) and re-optimized fully the atomic positions in the built heterostructures. To quantitatively understand the stability of the graphene/MTe heterostructures, we compute the binding energies (E_b) according to the following formula:[28]

$$E_b = \frac{(E_{graphene/MTe} - E_{graphene} - E_{MTe})}{m} \quad (1)$$

where $E_{graphene/MTe}$, $E_{graphene}$ and E_{MTe} are the total energies of the graphene/MTe heterostructures, graphene and MTe monolayers, respectively. m is the number of atoms in the studied 2D system, which is equal to 10 for graphene/AlTe and 34 for graphene/BTe. Based on the computed bonding energies (see Table 1 (ESI†)), the most stable structure of the graphene/AlTe heterostructures is type-I-stacking configuration, while the most stable structure of the graphene/BTe heterostructures is type-II-stacking configuration. Thus, the type-I-stacking graphene/AlTe and type-II-stacking graphene/BTe heterostructures are mainly discussed in the following section. The binding energies for type-I-stacking graphene/AlTe and type-II-stacking graphene/BTe are −359.43 meV and −150.87 meV, respectively.

Published on 27 June 2019. Downloaded by Radboud University Nijmegen on 8/13/2019 10:43:32 AM.

Compared with the binding energy (−60 meV) of the graphene/phosphorene heterostructures,[29] the considered graphene/MTe heterostructures have much lower binding energies and have more strong vdW interactions, indicating that fabricating a graphene/MTe system is feasible in the experiment. The equilibrium distances, marked by D, at 3.55 Å and 3.68 Å are most stable in energy for graphene/AlTe and graphene/BTe heterostructures, respectively. The values of D are similar to that of other graphene-based heterostructures,[30–32] which are typical in the vdW heterostructures. For instance, the interlayer distance of the graphene/MoS_2 vdW heterostructures is 3.40 Å.[17] The equilibrium distance in the graphene/SnS vdW heterostructures is 3.32 Å.[3] The weak vdW interaction therefore exists in graphene/MTe.

Electronic structures of graphene/MTe heterostructures

We now explore the electronic structures of the graphene/MTe vdW heterostructures at the ground state by plotting the band structures of graphene, AlTe and BTe monolayers and graphene/MTe heterostructures. It is observed from Fig. 2(a) and (d) that graphene has a zero band gap and possesses a linear Dirac cone-like structure around the Fermi level. Moreover, the Dirac cone-like structure of graphene exists at the Γ-point, as expected. Fig. 2(b) and (e) show that AlTe and BTe are indirect semiconductors with the band gaps of 1.68 eV and 1.52 eV, respectively. These calculated results are consistent with the previous report (1.74 eV for AlTe and 1.52 eV for BTe).[21] Moreover, the PBE method always underestimates the band gap of semiconductors. The Heyd–Scuseria–Ernzerhof (HSE) method is often used to correct the gap values and band edges.[33] The band gaps of AlTe and BTe with HSE06 are 2.24 and 2.18 eV, respectively, and the corresponding band structures are shown in Fig. S4(a and b) (ESI†), respectively. HSE requires extremely expensive computational costs, and the trends in physical properties can be accurately described by using the PBE method. Therefore, in this work, all electronic properties of graphene/XTe heterostructures under out-of-plane strains and electric fields are calculated with PBE. The projected band structures of the graphene/AlTe and graphene/BTe heterostructures are shown in Fig. 2(c) and (f), respectively. Here, orange, gray and magenta symbols represent graphene, AlTe and BTe, respectively. It is obvious that the band structure of the heterostructures is the simple sum of each constituent. The Dirac cone-like structure of graphene remains intact around the Fermi level. The band shapes and values of the band gap of MTe remain unchanged. These features mentioned above indicate further that the weak vdW interaction exists in the graphene/MTe heterostructures.

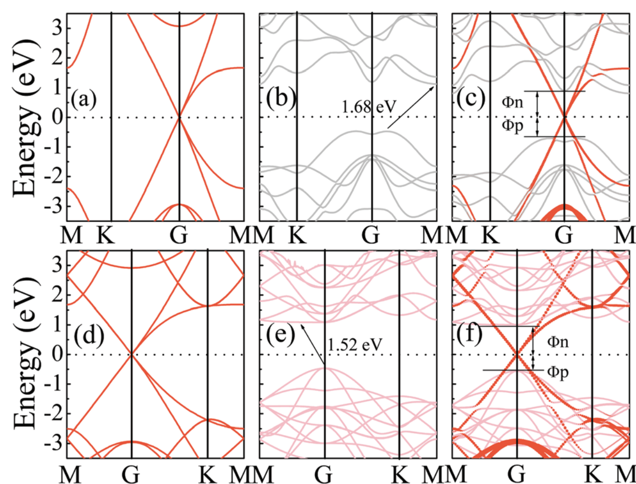

Fig. 2 The band structures of (a) $\sqrt{3} \times \sqrt{3} \times 1$ graphene, (b) 1 × 1 × 1 AlTe, (c) graphene/AlTe heterostructures, (d) 3 × 3 × 1 graphene, (e) 2 × 2 × 1 BTe and (f) graphene/AlTe heterostructures.

Similar to graphene-based semimetal–semiconductor heterostructures, such as graphene/arsenene,[34] graphene/black phosphorene[35] and graphene/MoSeS,[36] the graphene/MTe heterostructures form Schottky barriers at interfaces. As shown in Fig. 2(c) and (f), for the graphene/MTe heterostructures, the Fermi level located at the Dirac point is close to the valence band of MTe, as a result of which p-type Schottky barriers are formed at the graphene/AlTe and graphene/BTe interfaces with 0.72 and 0.49 eV, respectively.

In practice, a tunable SBH is very important in the electronic device applications.[37,38] We thus tune the position of the Dirac point of graphene with respect to the band edge of MTe by adjusting the interlayer distance D between graphene and MTe. This method, applying out-of-plane strains, can effectively control the SBH of graphene-based vdW heterostructures and be achieved in the experiment *via* vacuum thermal annealing,[39] nano-mechanical pressure[5] and so on.[40,41] We firstly calculate the electronic structures of the graphene/AlTe heterostructures with different interlayer distances. Fig. 3(a–c) show projected band structures with the selected interlayer distances (D = 2.55, 2.95 and 4.55 Å). As the interlayer distance is 4.55 Å, the Dirac point of graphene is close to the CBM of AlTe, forming an n-type Schottky contact at the graphene/AlTe interfaces. Compared with Φ_p (0.72 eV) at an equilibrium interlayer distance, Φ_p (0.27 eV) at D = 2.95 Å gets smaller. Interestingly, when D = 2.55 Å, the Dirac point of graphene disappears, and the graphene/AlTe heterostructures become semiconductors with the type-II band alignment and a band gap of 0.19 eV.

Fig. 3(d) shows the evolution of binding energies as a function of the interlayer distances. The lowest stability of the graphene/AlTe heterostructures is found at D = 3.55 Å, similar to the previous calculated value in this work. Fig. 3(e) shows the SBH of graphene/AlTe as a function of the interlayer distance. As the interlayer distance decreases, Φ_p gradually decreases while Φ_n increases, forming a crossover at D = 3.75 Å and achieving a transition from a p-type Schottky to n-type Schottky contact. When the interlayer distance decreases to 2.60 Å, the graphene/AlTe heterostructures become semiconductors. The reason is that the graphene/AlTe heterostructures with a large compressive strain makes the two carbon sublattices inequivalent. The sublattice-symmetry-breaking generates directly an intrinsic and robust mass for the Dirac fermions, inducing a band gap.[42] Such physical

 This journal is © The Royal Society of Chemistry 2019

Published on 27 June 2019. Downloaded by Radboud University Nijmegen on 8/13/2019 10:43:32 AM.

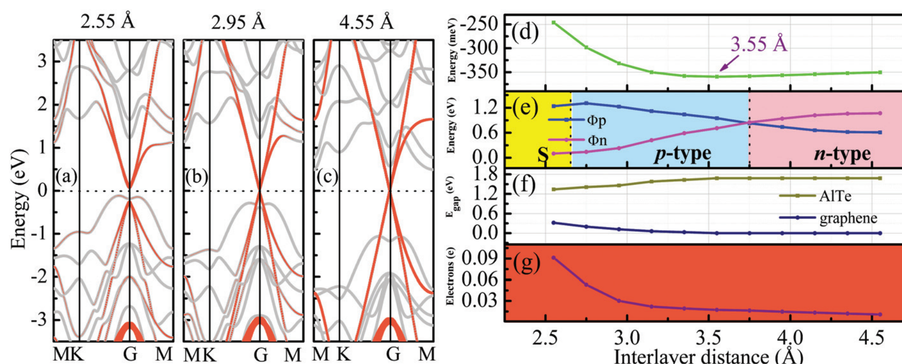

Fig. 3 (a–c) The projected band structures of the graphene/AlTe heterostructures at interlayer distances of D = 2.55, 2.95 and 4.55 Å. Orange and gray symbols represent graphene and AlTe, respectively. (d) The variation of the binding energies, (e) the evolution of Schottky barriers, (f) the band gap of graphene and AlTe and (g) transferred electrons from graphene to AlTe in the graphene/AlTe heterostructures as a function of the interlayer distance.

phenomena are found in other vdW heterostructures, such as graphene/h-BN,[8] MoS_2/h-BN/graphene.[43] The band gaps as a function of the applied out-of-plane strains is plotted in Fig. 3(f). The applied tensile strain has little influence on the band gap. However, as the strength of the applied compressive strain increases, the band gap of the graphene (AlTe) monolayer increases (decreases). This can be explained based on the fact that compressive strains destroy slightly the vdW interaction between graphene and AlTe, as a result of which graphene and AlTe monolayer cannot retain independently its intrinsic electronic properties.

To deeply explore the mechanism of the applied out-of-plane strain effect on the evolution of the Schottky barrier, we plotted the charge density difference of the graphene/AlTe heterostructures at an equilibrium distance (see Fig. S6(a) and (c) (ESI†)) and computed the number of electrons that flow from graphene to AlTe according to the Bader charge analysis.[4] It can be seen from Fig. 3(g) that when the interlayer distance decreases, more and more electrons transfer from graphene to AlTe monolayer. As a consequence, the position of the Dirac point of graphene moves towards the valence band of AlTe. Intrinsic p-type transforms into an n-type Schottky contact at the graphene/AlTe interfaces until the interlayer distance reduces to a critical value (2.60 Å).

Fig. S5(a–g) (ESI†) exhibit the corresponding electronic structures of the graphene/BTe heterostructures under different applied out-of-plane strains. The results present that the electronic structures are similar to the graphene/AlTe heterostructures. The only difference is that the evolution of the SBH is more insensitive to the applied out-of-plane strain in the graphene/BTe heterostructures. For instance, a transition occurs under a tensile strain of 0.53 Å from a p-type to n-type Schottky contact at the graphene/BTe interfaces, larger than that under a tensile strain of 0.19 Å at the graphene/AlTe interfaces, as shown in Fig. 3(e) and Fig. S5(e) (ESI†). The results imply that the modulated SBH in the graphene/MTe heterostructures can tune the contact resistance by applying an appropriate out-off-plane strain.

From the above discussed results, electrons flow from graphene to MTe monolayers, creating an interface dipole, defined by a potential step (ΔV) at the graphene/MTe interfaces (see Fig. 4).[44] Considering the influence of ΔV on the Schottky–Mott rule, the SBH should be re-written as formula (2), then the calculated SBH will be in agreement with the values measured in the experiment.

$$\begin{aligned} \Phi_n &= W_{graphene} + \Delta V - \chi_{graphene\text{-}MTe} \\ \Phi_p &= I_{graphene\text{-}MTe} - (W_{graphene} + \Delta V) \end{aligned} \qquad (2)$$

here, $W_{graphene}$ is the work function of graphene. $\chi_{graphene\text{-}MTe}$ and $I_{graphene\text{-}MTe}$ are the electron affinity and ionization potential of graphene-MTe, respectively. ΔV is defined as ΔV = $W_{graphene\text{-}MTe}$ − $W_{graphene}$, and W_{XTe} is the work function of MTe. The calculated value of ΔV is essentially determined by the number of electron transfer: the more the electron transfers, the larger the interface dipole and ΔV. In this work, the work functions of graphene, AlTe and BTe are calculated to be 4.21, 4.88 and 4.23 eV, respectively. At the equilibrium distance, the work functions of graphene/AlTe and graphene/BTe are 4.92 and 4.29 eV, respectively. $\chi_{graphene\text{-}AlTe}$, $I_{graphene\text{-}AlTe}$, $\chi_{graphene\text{-}MTe}$ and $I_{graphene\text{-}BTe}$ are computed to be 3.49, 5.17, 3.34 and 4.86 eV, respectively. Based on formula (2), Φ_n and

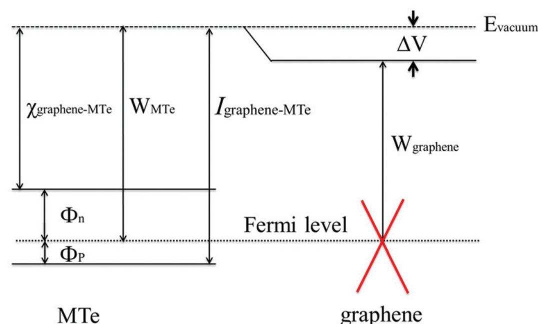

Fig. 4 The band diagram in the graphene/MTe heterostructures.

Published on 27 June 2019. Downloaded by Radboud University Nijmegen on 8/13/2019 10:43:32 AM.

Φ_p of the graphene/AlTe heterostructures are 1.43 and 0.27 eV, respectively, and Φ_n and Φ_p of the graphene/BTe heterostructures are 0.95 and 0.57, respectively. These values of Φ_n or Φ_p are greatly different from the corresponding values without ΔV. Thus, the interface dipole at the graphene/MTe interfaces must be considered within the vdW interaction range. Nonetheless, as the interface electron redistribution becomes negligible at a large enough interlayer distance, graphene/MTe has the same work function as that of graphene, resulting in $\Delta V \approx 0$, thus Φ_n and Φ_p converge to $W_{graphene} - \chi_{XTe}$ and $I_{XTe} - W_{graphene}$, respectively. For instance, when the interlayer distance between graphene and AlTe is D = 4.55 Å, χ_{AlTe} and I_{AlTe} are calculated to be 3.25 and 4.93 eV, respectively. The converged Φ_n (Φ_p) of the graphene/AlTe heterostructures are further computed to be 0.96 (0.72) eV, agreeing with the values shown in Fig. 3(e).

In the experiments, graphene-based heterostructures as a building block works successfully in field effect transistors (FETs), such as MoS_2/h-BN/graphene[45] and graphene/MoS_2 [15] heterostructures. Therefore, the graphene-based heterostructures are always subjected to the applied electric fields. To understand the effect of the applied electric fields on the Schottky barrier, the SBHs are computed with different strengths of applied electric fields, and the positive direction of the electric fields is defined as the direction from MTe to graphene. The SBH in the graphene/AlTe heterostructures can be linearly tuned by the applied electric fields as shown in Fig. 5(e). We can see that when the applied negative electric fields decrease to −0.01 V Å^{-1}, a shift occurs from a p-type to n-type Schottky contact at the graphene/AlTe interfaces. More interestingly, when the applied negative electric field decreases to −0.15 V Å^{-1}, the n-type Schottky contact transforms into an Ohmic contact with a SBH of zero. When the applied positive electric fields increase to 0.14 V Å^{-1}, conversion from the p-type Schottky to Ohmic contact occurs.

Fig. 5(b) shows the projected band structure of the graphene/AlTe heterostructures under an applied electric field of −0.22 V Å^{-1}. The Dirac point of graphene lies above the Fermi level, resulting in p-type (hole) doping of graphene in the graphene/AlTe heterostructures. Moreover, the CBM of AlTe sinks below the Fermi level, forming an Ohmic contact at the graphene/AlTe interfaces. The evolution from a Schottky to Ohmic contact can be explained based on the fact that the charge carrier (electron) flows from AlTe to graphene. When an electric field of −0.12 V Å^{-1} is applied, the Dirac point of graphene is close to the CBM of AlTe, leading to the formation of an n-type Schottky contact, as shown in Fig. 5(c). On the other hand, we can see from Fig. 5(d) that under an applied electric field of 0.12 V Å^{-1}, the Dirac point of graphene is close to the VBM of AlTe, forming a p-type Schottky contact. Fig. 5(e) shows that when the applied electric field is 0.22 V Å^{-1}, the VBM of AlTe moves up and crosses the Fermi level and the Dirac point of graphene is located below the Fermi level, which implies that the Ohmic contact and n-type (electron) doping of graphene is found in the graphene/AlTe heterostructures, respectively. Therefore, the applied electric fields tune the contact formation (Schottky and Ohmic contacts) and the doping (hole or electron) of graphene in the graphene/AlTe heterostructures.

Here, the influence of the applied electric fields on the doping of graphene in the graphene/AlTe heterostructures is further studied. ΔE_D can describe the hole or electron doping type of graphene in the graphene/AlTe heterostructures, where ΔE_D is the difference between the Dirac point (E_D) of graphene and the Fermi level (E_F) ($\Delta E_D = E_D - E_F$). When $\Delta E_D > 0$ and the Dirac point of graphene is located above the Fermi level (E_F), the p-type (hole) doping of graphene is found. When $\Delta E_D < 0$ and the Dirac point of graphene is located below the Fermi level (E_F), the n-type (electron) doping of graphene is observed. In the inset of Fig. 6, one can see that when the strength of the applied electric fields is less than −0.12 V Å^{-1}, ΔE_D is larger than zero and increases linearly, the doping type of graphene in the graphene/AlTe heterostructures therefore is p-type. When the applied electric field is more than 0.12 V Å^{-1}, ΔE_D is less than zero and decreases linearly, so the doping type of graphene in the graphene/AlTe heterostructures is n-type.

Based on the linear dispersion around the Dirac point of graphene and by following eqn (3),[46] we investigate the influ-

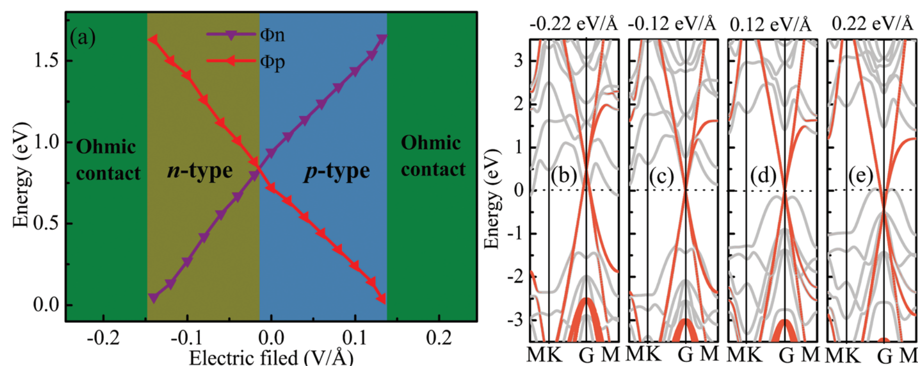

Fig. 5 Schottky barriers Φ_n and Φ_p in the graphene/AlTe heterostructures as a function of the applied electric field. (b–e) The projected band structures of the graphene/AlTe heterostructures under applied electric fields of −0.22, −0.12, 0.12 and 0.22 V Å^{-1}. Orange and gray symbols represent graphene and AlTe, respectively.

This journal is © The Royal Society of Chemistry 2019

Published on 27 June 2019. Downloaded by Radboud University Nijmegen on 8/13/2019 10:43:32 AM.

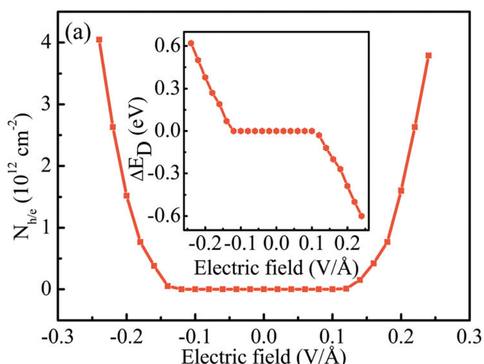

Fig. 6 The doping charge carrier concentration $N_{h/e}$ (10^{12} cm^{-2}) as a function of the applied electric fields in the graphene/AlTe heterostructures. The difference ΔE_D between the Dirac point of graphene and the Fermi level is plotted in the inset.

ence of the applied electric fields on the doping charge carrier (hole or electron) concentrations of graphene.

$$N_{h/e} = \frac{(\Delta E_D)^2}{\pi(\hbar v_F)^2} \quad (3)$$

as shown in Fig. 6, the doping charge carrier concentrations of graphene in the graphene/AlTe heterostructures maintain zero when the applied electric field ranges from −0.12 to 0.12 V Å^{-1}. However, when the applied electric field is less than −0.12 V Å^{-1} (or more than 0.12 V Å^{-1}), the doping charge carrier concentrations of graphene increase significantly, which can be up to 10^{12} cm^{-2} comparable to that of graphene/MoS_2.[17]

The effect of the applied electric fields on the contact formation (Schottky and Ohmic contacts) and the tunable doping of graphene in the graphene/AlTe heterostructures can be explained as follows. The applied electric fields affect the interface charge transfer in the graphene/AlTe heterostructures. From the previous calculated band structure of the graphene/AlTe heterostructures in this work (Fig. 2(c)), the Dirac point of graphene is almost located in the center of the band gap of AlTe in the graphene/AlTe heterostructures. The electrons that transfer between from the Dirac point of graphene to the CBM of AlTe and from the VBM of AlTe to the Dirac point of graphene need a little different strength of the applied electric fields. As a result, when the applied electric field is −0.22 V Å^{-1}, p-type (electron) doping of graphene is obtained in the graphene/AlTe heterostructures, and the doping charge carrier concentration is as high as 2.7×10^{12} cm^{-2}. When the applied electric field is 0.22 V Å^{-1}, n-type (electron) doping of graphene is deserved in the graphene/AlTe heterostructures, and the doping charge carrier concentration is unchanged.

The corresponding properties of the graphene/BTe heterostructures under the applied electric fields are exhibited in Fig. S7(a–g) and S8 (ESI†). The results are also similar to that of the graphene/AlTe heterostructures. Notably, an applied negative electric field of −0.65 V Å^{-1} can achieve a shift from a p-type to n-type Schottky contact at the graphene/BTe interfaces. When the applied negative electric field decreases to −0.21 V Å^{-1}, the n-type Schottky contact transforms into the Ohmic contact. When the applied positive electric field increases to 0.09 V Å^{-1}, the p-type Schottky contact transforms into the Ohmic contact. Thus, the electronic structures of the graphene/BTe heterostructures are more insensitive to the applied positive electric fields, compared with that of the graphene/AlTe heterostructures. The reason for this phenomenon is that the Dirac point of graphene is closer to the CBM of AlTe than the VBM of AlTe, as shown in the projected band structure of the graphene/AlTe heterostructures (Fig. 2(f)).

Conclusions

In summary, we investigated the geometry and electronic structures of the novel graphene/MTe heterostructures. Our density functional calculations imply that the weak vdW interaction exists in graphene/MTe. The p-type Schottky barriers are formed at the graphene/AlTe and graphene/BTe interfaces with 0.72 and 0.49 eV, respectively. Additionally, as the interlayer distance decreases, more and more electrons transfer from graphene to MTe monolayers. As a consequence, the position of the Dirac point of graphene shifts towards the valence band of MTe. An intrinsic p-type Schottky contact transforms into an n-type Schottky contact at the graphene/MTe interfaces, until the interlayer distance reduces to the critical value (2.60 Å for graphene/MTe and 2.88 Å for graphene/BTe).

In addition, for the graphene/AlTe heterostructures, an applied negative electric field decreases to −0.01 V Å^{-1}, and a shift occurs from the p-type to n-type Schottky contact in the graphene/AlTe heterostructures. When an applied negative electric field decreases to −0.15 V Å^{-1} or an applied positive electric field increases to 0.14 V Å^{-1}, the conversion from the p-type Schottky to Ohmic contact takes place. Interestingly, the hole doping of graphene in the graphene/AlTe heterostructures can be achieved as an applied electric field is less than −0.12 V Å^{-1}. When an applied electric field is more than 0.12 V Å^{-1}, the doping type is electron doping of graphene. Moreover, an applied electric field can modulate the charge carrier concentrations, which can be tuned up to 10^{12} cm^{-2}. For the graphene/AlTe heterostructures, its electronic structures are similar to that of the graphene/AlTe heterostructures. We believe that our results provide potential guidance towards graphene/MTe heterostructure-based electronic devices.

Conflicts of interest

The authors declare no competing financial interest.

Acknowledgements

This work was supported by the National Key Research and Development Plan (MOST) under Grant Number 2017YFA0205802 and the NSFC under Grant Number 11574235.

Published on 27 June 2019. Downloaded by Radboud University Nijmegen on 8/13/2019 10:43:32 AM.

References

1 R. Raccichini, A. Varzi, S. Passerini and B. Scrosati, *Nat. Mater.*, 2015, **14**, 271–279.
2 S. Stankovich, D. A. Dikin, G. H. Dommett, K. M. Kohlhaas, E. J. Zimney, E. A. Stach, R. D. Piner, S. T. Nguyen and R. S. Ruoff, *Nature*, 2006, **442**, 282.
3 X. Li and L. Zhi, *Chem. Soc. Rev.*, 2018, **47**, 3189.
4 C. Xia, L. Fang, X. Li, W. Xiong and Z. Geng, *J. Alloys Compd.*, 2018, **766**, 215–220.
5 M. Dienwiebel, G. S. Verhoeven, N. Pradeep, J. W. M. Frenken, J. A. Heimberg and H. W. Zandbergen, *Phys. Rev. Lett.*, 2004, **92**, 126101.
6 K. D. Pham, N. N. Hieu, H. V. Phuc, I. A. Fedorov, C. A. Duque, B. Amin and C. V. Nguyen, *Appl. Phys. Lett.*, 2018, **113**, 171605.
7 L. Yu, Y.-H. Lee, X. Ling, E. J. Santos, Y. C. Shin, Y. Lin, M. Dubey, E. Kaxiras, J. Kong and H. Wang, *Nano Lett.*, 2014, **14**, 3055–3063.
8 A. Ramasubramaniam, D. Naveh and E. Towe, *Nano Lett.*, 2011, **11**, 1070.
9 G. H. Lee, Y. J. Yu, X. Cui, N. Petrone, C. H. Lee, M. S. Choi, D. Y. Lee, C. Lee, W. J. Yoo and K. Watanabe, *ACS Nano*, 2013, **7**, 7931–7936.
10 Q. Wu, S. K. Jang, S. Park, S. J. Jung, H. Suh, Y. H. Lee, S. Lee and Y. J. Song, *Nanoscale*, 2015, **7**, 7574.
11 C. Xia, B. Xue, T. Wang, Y. Peng and J. Yu, *Appl. Phys. Lett.*, 2015, **107**, 666.
12 J. Bardeen, *Phys. Rev.*, 1947, **71**, 717–727.
13 M. Sun, J. P. Chou, J. Yu and W. Tang, *Phys. Chem. Chem. Phys.*, 2017, **19**, 17324.
14 S. Tongay, T. Schumann, X. Miao, B. R. Appleton and A. F. Hebard, *Carbon*, 2011, **49**, 2033–2038.
15 L. Britnell, R. V. Gorbachev, R. Jalil, B. D. Belle, F. Schedin, A. Mishchenko, T. Georgiou, M. I. Katsnelson, L. Eaves and S. V. Morozov, *Science*, 2012, **335**, 947–950.
16 W. Hu, Z. Li and J. Yang, *J. Chem. Phys.*, 2013, **138**, 197.
17 W. Hu, T. Wang, R. Zhang and J. Yang, *J. Mater. Chem. C*, 2016, **4**, 1776–1781.
18 W. Xiong, C. Xia, X. Zhao, T. Wang and Y. Jia, *Carbon*, 2016, **109**, 737–746.
19 C. Xia, Q. Gao, W. Xiong, J. Du, X. Zhao, T. Wang, Z. Wei and J. Li, *J. Mater. Chem. C*, 2017, **5**, 7230–7235.
20 P. Hu, L. Wang, M. Yoon, J. Zhang, W. Feng, X. Wang, Z. Wen, J. C. Idrobo, Y. Miyamoto and D. B. Geohegan, *Nano Lett.*, 2013, **13**, 1649–1654.
21 S. Demirci, N. Avazlı, E. Durgun and S. Cahangirov, *Phys. Rev. B*, 2017, **95**, 115409.
22 G. Kresse, *Phys. Rev. B: Condens. Matter Mater. Phys.*, 1996, **54**, 11169.
23 G. Kresse, *Comput. Mater. Sci.*, 1996, **6**, 15.
24 J. P. Perdew, K. Burke and M. Ernzerhof, *Phys. Rev. Lett.*, 1996, **77**, 3865.
25 S. Grimme, *J. Comput. Chem.*, 2006, **27**, 1787–1799.
26 D. Zhang, Z. Zhou, H. Wang, Z. Yang and C. Liu, *Nanoscale Res. Lett.*, 2018, **13**, 400.
27 C. Mondal, S. Kumar and B. Pathak, *J. Mater. Chem. C*, 2018, **6**, 1920–1925.
28 A. Samad, M. Noor-A-Alam and Y. H. Shin, *J. Mater. Chem. A*, 2016, **4**, 14316.
29 J. Padilha, A. Fazzio and A. J. da Silva, *Phys. Rev. Lett.*, 2015, **114**, 066803.
30 S. Li, M. Sun, J.-P. Chou, J. Wei, H. Xing and A. Hu, *Phys. Chem. Chem. Phys.*, 2018, **20**, 24726–24734.
31 H. V. Phuc, N. N. Hieu, B. D. Hoi and C. V. Nguyen, *Phys. Chem. Chem. Phys.*, 2018, **20**, 17899–17908.
32 Z. Ben Aziza, H. Henck, D. Pierucci, M. G. Silly, E. Lhuillier, G. Patriarche, F. Sirotti, M. Eddrief and A. Ouerghi, *ACS Nano*, 2016, **10**, 9679–9686.
33 P. Le, L. M. Bui, N. N. Hieu, H. V. Phuc, B. Amin, N. V. Hieu and C. V. Nguyen, *Diamond Relat. Mater.*, 2019, **94**, 129–136.
34 Y. Wang and Y. Ding, *Phys. Chem. Chem. Phys.*, 2015, **17**, 27769–27776.
35 W. Hu, T. Wang and J. Yang, *J. Mater. Chem. C*, 2015, **3**, 4756–4761.
36 K. D. Pham, N. N. Hieu, H. V. Phuc, B. D. Hoi, V. V. Ilysov, B. Amin and C. V. Nguyen, *Comput. Mater. Sci.*, 2018, **153**, 438–444.
37 E. Sanville, S. D. Kenny, R. Smith and G. Henkelman, *J. Comput. Chem.*, 2007, **28**, 899–908.
38 D. Zhang, Z. Zhou, Y. Hu and Z. Yang, *Mater. Res. Express*, 2018, **6**, 035513.
39 S. Tongay, W. Fan, J. Kang, J. Park, U. Koldemir, J. Suh, D. S. Narang, K. Liu, J. Ji and J. Li, *Nano Lett.*, 2014, **14**, 3185.
40 S. M. Clark, K. J. Jeon, J. Y. Chen and C. S. Yoo, *Solid State Commun.*, 2013, **154**, 15–18.
41 H. Fang, C. Battaglia, C. Carraro, S. Nemsak, B. Ozdol, J. S. Kang, H. A. Bechtel, S. B. Desai, F. Kronast and A. A. Unal, *Proc. Natl. Acad. Sci. U. S. A.*, 2014, **111**, 6198–6202.
42 G. Giovannetti, P. A. Khomyakov, G. Brocks, P. J. Kelly and J. V. D. Brink, *Phys. Rev. B: Condens. Matter Mater. Phys.*, 2007, **76**, 3009–3014.
43 W. Zan, W. Geng, H. Liu and X. Yao, *Phys. Chem. Chem. Phys.*, 2016, **18**, 3159–3164.
44 B. Liu, L. J. Wu, Y. Q. Zhao, L. Z. Wang and M. Q. Cai, *Phys. Chem. Chem. Phys.*, 2016, **18**, 19918.
45 G. H. Lee, Y. J. Yu, C. Xu, N. Petrone, C. H. Lee, S. C. Min, D. Y. Lee, C. Lee, W. J. Yoo and K. Watanabe, *ACS Nano*, 2013, **7**, 7931–7936.
46 W. Hu, Z. Li and J. Yang, *J. Chem. Phys.*, 2013, **138**, 197.

 This journal is © The Royal Society of Chemistry 2019